Electronic Supplementary Material (ESI) for Lab on a Chip.

Micropatterned biofilm formations by laminar flow-templating

Nahid Babaei Aznaveh,[a] Muhammad Safdar,[a,b] Gideon Wolfaardt[c] and Jesse Greener*[a]

[a] Département de Chimie, Université Laval, 1045 Avenue de la Médecine, Québec, QC G1V 0A6, Canada.

[b] Department of Chemistry, University of Eastern Finland, Yliopistokatu 7, FI-80101 Joensuu, Finland.

[c] Department of Chemistry and Biology, Ryerson University, 350 Victoria Street, Toronto, ON, M5B 2K3, Canada., and Department of Microbiology, Stellenbosch University, Private Bag X1, Stellenbosch, 7602, South Africa

* Correspondence should be sent to: Fax/Tel: 418 656-7916, 418-656-2131 x 7157, E-mail: jesse.greener@chm.ulaval.ca

1) Reducing the effect of diffusion on template streams

In order optimise the stability of the template pattern over long distances, we sought to minimise the diffusive mixing, which, according to Fick's law is proportional to solute diffusivity, D, and the local concentration gradient. Diffusivity of small molecules and ions such as Na^+ (D_{Na^+} = 1.3 x10^{-9} $m^2 \cdot s^{-1}$) or Cl^- (D_{Cl^-} = 2.0 x10^{-9} $m^2 \cdot s^{-1}$) used in high concentrations in growth solutions, can be significant in comparison to citrate diffusivity of 6.9x10^{-10} $m^2 \cdot s^{-1}$. Furthermore, concentration gradients between the confinement stream and the biofilm precursor template streams can be high due to excellent flow separation in microchannels due to low Reynold's numbers. Together, these two factors could result in a large flux of molecules out of the biofilm precursor template stream into the confinement stream since the confinement stream did not contain the same highly diffusive species. Moreover, a large flux of highly diffusive molecules can result in the mass-transfer of other, less diffusive, co-dissolved molecules and suspended bacteria. This effect caused the width of the template solution (w_T) to expand as it moved down

the measurement channel. Preliminary experiments using pure water as the confinement stream, s_C, always resulted in large mass transfer from the biofilm precursor stream (Fig S1a). One approach to minimise variations in w_T was to increase the total flow rate without altering the flow rate ratio Q_C/Q_T. This had the effect of limiting the time for diffusion while in the measurement channel because at high velocity carried the liquid flowed through the channel too quickly before diffusion could carry many particles out of the template stream. However, this approach would prevent the utilisation of low flow velocities, which are necessary in order to probe the effect of a wide variety of flow conditions on biofilm growth rates and their properties. A second approach was to reduce the concentration gradients between confinement and template streams. This was accomplished by adding the same solutes with the same concentration to the confinement stream, which were present in the template stream, with the exception of the carbon source (citrate), which is required to support biofilm growth. As a result, diffusion was visibly reduced, which resulted in the persistence of linear template streams down the entire measurement channel even at slow flow rates Figure S1b. We use the familiar calculation of the Péclet (Pe) number to estimate the channel distance required for complete mixing in the z and x directions for the slowest flow rate ($v = 0.36$ mm·s^{-1}) used in this study (T. M. Squires, S. R. Quake, Microfluidics: Fluid physics at the nanoliter scale Rev. Mod. Phys., 2005, 77, 977-1026). Calculated for citrate ($D = 6.9 \times 10^{-10}$ m^2·s^{-1}) in the z-direction, using $Pe_z = v \cdot s\ h_M/D$ and x-direction using $Pe_x = v \cdot s\ w_M/D$, with h_M = 0.35mm and w_M = 2mm, we determined diffusion lengths needed for complete mixing in these two directions should be 0.35 m and 1 m long, respectively. Since the measurement channel length is only 10 mm long, we conclude that the citrate molecules are strongly

localized in the template stream throughout the entire length of the measurement channel.

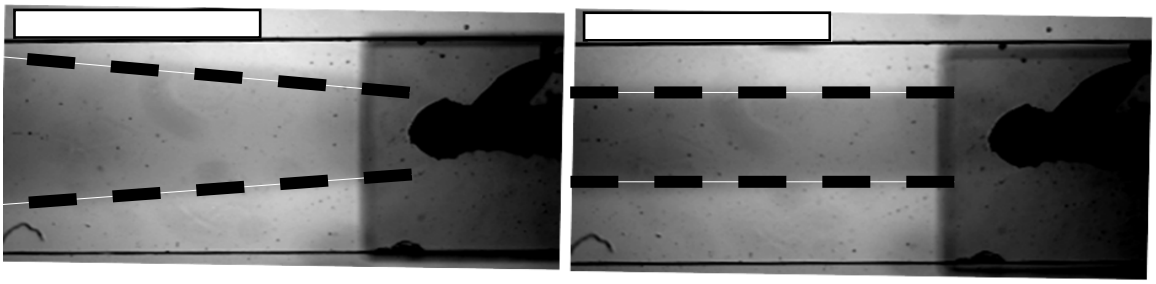

Fig. S1 (a) Transmission image of a poorly confined template solution in the measurement channel in during injection of confinement fluid consisting of pure water flowing at $Q_C = 0.5$ mL·h^{-1} and the dye containing template solution $Q_T = 0.3$ mL·h^{-1}. (b) An image of a well-confined template solution due to new confinement stream composition as discussed in the main text above. Flow conditions in (b) were the same as (a). Heavy dashed lines highlight the interface between the template and confinement streams. White boxes on the top left of the image (a) and (b) are scale bars with length 2000 μm. Flow is from right to left in both figures.

2) Flow templated biofilm inoculation

The growth of biofilms in the measurement channel began with flow-templated inoculation of the FT-μBR using a solution containing suspended CT07-GFP bacteria. Figure S2a shows a transmission microscope image taken during this process. From the junction output, at the right of the image, a visible stream of planktonic-phase CT07 bacteria co-flowed downstream in a linear pattern, confined by a transparent confinement stream. Flow rates for the confinement and template flow were $Q_C = 0.3$ mL·h^{-1} and $Q_T = 1.75$ mL·h^{-1}, respectively. This stream is fed by the small channel from Level 2 (see main paper Figure 1). Figure S2b shows the same field of view under the same flow conditions taken in fluorescent mode, demonstrating that fluorescent bacterial cells were contained within the template phase. Here both the stream and Level 2 channel were bright due to the presence of fluorescent CT07-GFP.

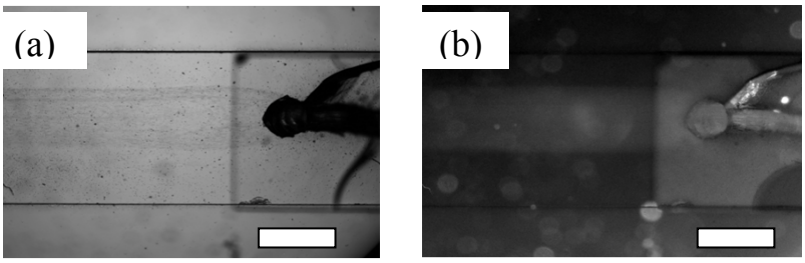

Fig. S2 (a) transmission image of the measurement channel in the vicinity of the junction during inoculation. Bacterial laden inoculant can be seen exiting the junction travelling downstream with flow rate Q_C = 1.75 mL·h^{-1}, Q_T = 0.3 mL·h^{-1} (b) Fluorescent mode image of the same region in (a), under the same flow conditions. The green fluorescent bacteria (CT07-GFP) are visible in the template flow stream and the Level 2 channel. Scale bar is 1000 μm. Flow is from right to left.

3) Microjunction fabrication parameters and their effect on the template stream

The effect that the angle between the junction hole and the measurement channel, θ, had on the template stream dimensions was determined by simulation for different flow rate ratios (Figures S3a and S3b). We noted a competing effect between the $w_T|_\theta$ and $h_T|_\theta$ in the range 35 > θ > 90. As θ decreased, the w_T increased gently from $w_{T|\theta=90^o}$ = 705 μm to $w_{T|\theta=45^o}$ = 725 μm for all Q_C/Q_T, but drastically increased for θ < 45 degrees. On the other hand, $h_{T|\theta}$ continuously decreased with decreasing θ, with a difference between $h_T|_{35o}$ and $h_T|_{90o}$ of approximately 15 μm at Q_C/Q_T = 10. In the case of both w_T and h_T, the difference in values for θ = 90^o and θ = 35^o was maximum at high flow rate ratios. Since our goal was to maximise the confinement of the template stream in the vertical and horisontal dimensions, we chose the median value of θ = 45^o. Computer simulations predict that w_T is particularly sensitive to the diameter of the microjunction (Figure S3c). However, this factor was not extensively explored experimentally because our fabrication process was limited by the availability of a single standardised PDMS punch that resulted in cylindrical junctions with diameter, d = 450 μm.

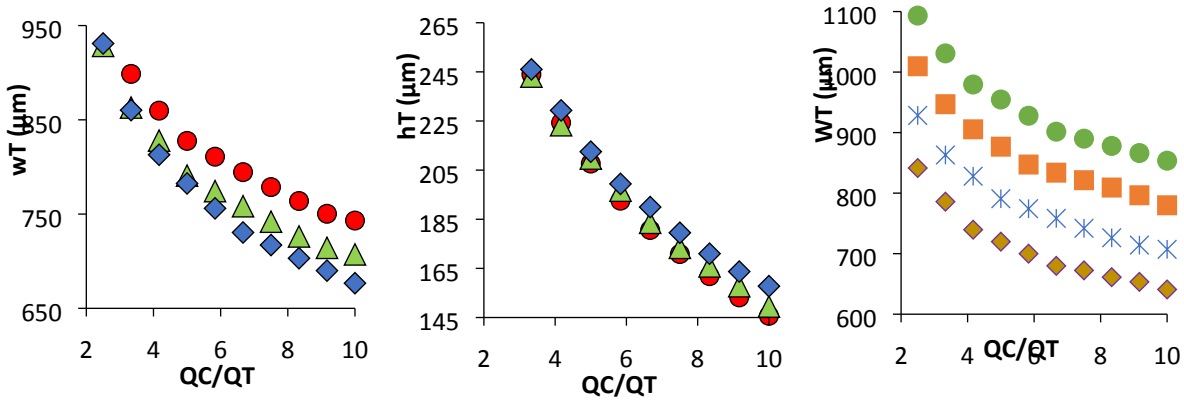

Fig. S3 (a) w_T vs. Q_C/Q_T and (b) h_T vs. Q_C/Q_T. For junction angles: 35° (red circles), 45° (green triangles), and 90° (blue diamonds). Inlet diameter was 450 µm for all simulations in (a) and (b). (c) w_T vs. Q_C/Q_T for junctions with widths: 400 µm (purple diamonds), 450 µm (blue asterisks), 500 µm (red squares), 550 µm (orange circles). All junction angles in (c) were 45°.

4) Template profiles determined by flow rate ratio, independent of total flow rate

Figure S4 shows flow profiles along the x-axis 800 µm downstream from the junction which had properties of θ = 45°, d = 450 µm. The superimposed template flow cross-section profiles show results for experiments and simulations for flow rate ratio of Q_C/Q_T = 10 collected at two different flow rate pairs: $Q_{C,1}$ = 3.0 mL·h^{-1}, $Q_{T,1}$ = 0.3 mL·h^{-1} and $Q_{C,2}$ = 6.0 mL·h^{-1}, $Q_{T,2}$ = 0.6 mL·h^{-1}. The two flow rates gave the same w_T and h_T despite having different total flow rates. A simulation of the heights confirms the dimensions to be expected.

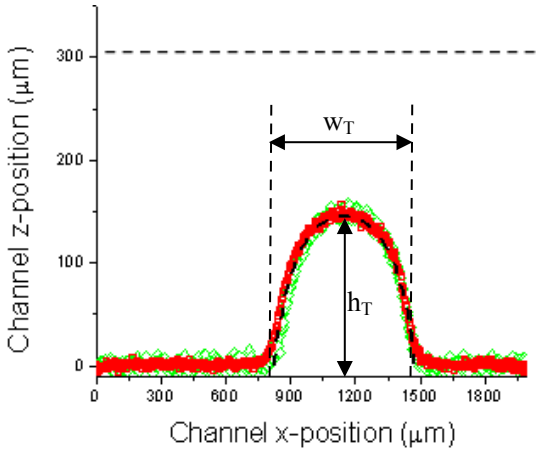

Fig. S4 Flow profile at a position 800 µm downstream of the junction for dye containing solution flowing with flow rates Q_C = 3.0 mL·h^{-1}, Q_T = 0.3 mL·h^{-1}.(red) and Q_C = 6.0 mL·h^{-1}, Q_T = 0.6 mL·h^{-1} (green). Black dashed line shows a simulation for the same flow rate ratio Q_C/Q_T = 10.

5) Biofilm colony counting

Individual biofilm colonies that appeared in microscope images were counted using image analysis software. A macro was written that analysed each image in a time-series data set, which converted 16-bit grey scale images to monochromatic images that identify and count individual biofilm colonies. The macro consisted of steps for background elimination and contrast enhancement with an automatic threshold adjustment. In some cases where devices were reused and remnants of former (non-living) biofilms were present, a background subtraction was applied. An example of the original image and the contrast enhanced image showing detected colonies is shown in Figure S5a and S5b, respectively. The number of colonies was automatically registered for each image in the time-series so that the number of colonies with respect to time could be tracked. See Figure S6 for an example. The technique is limited to the visible colonies, which in this study were relatively large due to the low power objective used (2x).

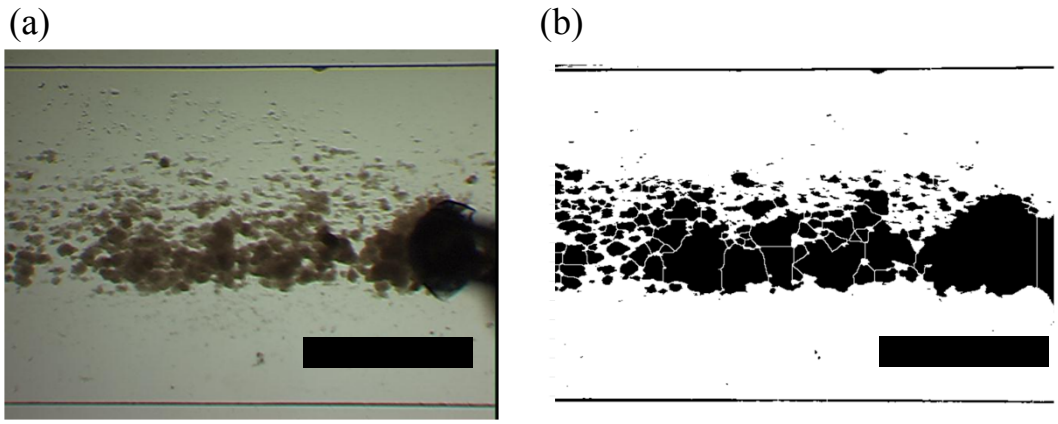

Fig. S5 (a) Greyscale microscope image of the biofilm grown under flow rates Q_C = 0.5 mL·h^{-1}, Q_T = 0.3

mL·h^{-1}. (b) High contrast image showing isolated colonies as detected by the image analysis macro. Flow was from right to left. Scale bar is 1000 µm.

6) Relation between the number of biofilm colonies and biomass density

Comparing the changes to biomass density with the number of colonies can be informative from the perspective of understanding the mechanisms at play during initial stages of biofilm growth. Figure S6 shows the pixel intensity from in data shown in Figure 6b (main paper) with the colony count superimposed on the same time scale. As can be seen, the number of individually resolved colonies is a maximum near 45 h after inoculation. This is the approximate time for the transition from rapid growth to mature growth phase (see main paper for details).

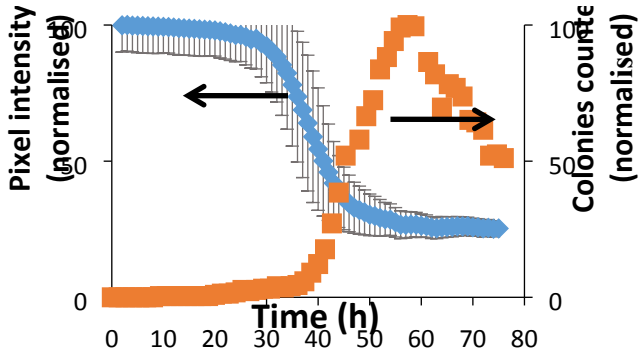

Fig. S6 Pixel intensity data set from Fig. 5b in main paper (blue diamonds) with results of colony counting superimposed on the same time scale (orange squares).

7) Biofilm growth under varied shear stress

A) Growth rate

As discussed in the main text, the slope of the rate of increase of optical density plot with time is nearly linear during the growth phase. Figure S7b shows relationship between slope of the growth curves and the applied shear stresses. As optical density and biomass density are proportional, but the proportionality constant is unknown, the y-axis values are arbitrary.

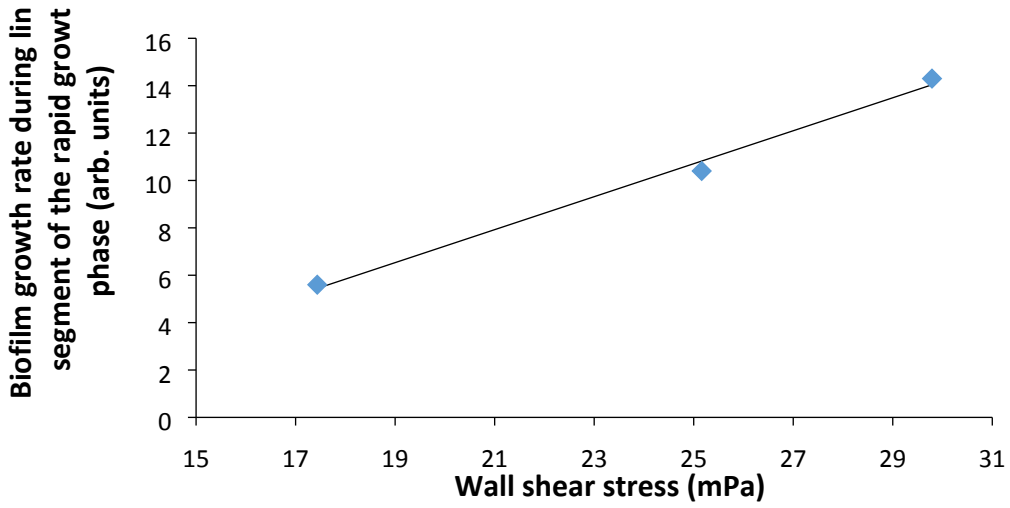

Fig. S7a Relation between change in the optical density (proportional to biofilm growth rate) and the applied wall shear stress. A linear trend line is fit to the data points.

B) **Lag time**

We noted a lag phase between inoculation and the observation of measurable biofilm development (*via* increases to optical density in bright field microscope images). We observed a linear relationship between the time duration of the lag phase (t_{lp}) and the wall shear stresses in the range of 17 to 30 mPa, which were applied to the FT-μBR during cultivation (Figure S7b). As noted in the main text we attribute this to the increasing time required for surface modification by the bacteria in order to enhance wall adhesion in shear flow environments.

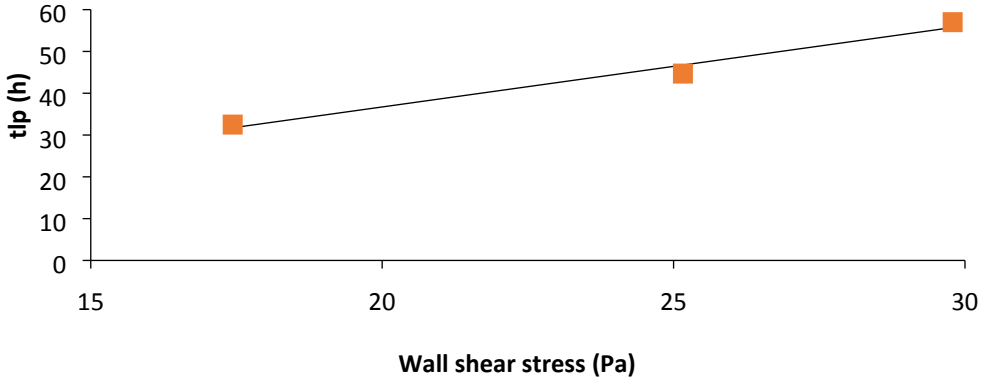

Fig S7b Relation between the length in time of the lag phase and the wall shear stress. Slope was

found by fitting linear trend line which had slope of 1.9 $h \cdot mPa^{-1}$.

8) Development of pre-biofilm phase sessile bacteria

As noted above, the lag phase between inoculation and the biofilm growth is likely due to the time required for surface conditioning by the bacteria to achieve good adhesion in the increasing shear flow environment. To monitor bacterial growth in advance of observable changes to low resolution optical density experiments described in the main paper, we used a high numerical aperture (0.9), high magnification (100x) objective. We monitored the growth of the pre-biofilm sessile bacteria against the FT-μBR glass coverslip in an unconfined template stream of media solution containing citrate concentration of 10 mM. Figure 8a is comprised of micrographs of bacteria at the adhesion surface at different times after inoculation, for the flow rate $Q_{Tot} = 0.17$ $mL \cdot h^{-1}$. We used software-based cell counting macros to determine the number of bacteria in the field of view with time until it became difficult to resolve individual bacteria, due to significant growth out of the focal plane . Using this counting method, we obtained the curves in Figures S8b. As seen in the micrographs in Figure S8a, cell density remained low for an initial period and then increased rapidly until biofilms could be seen via changes to optical density. We note that the initial time during which the bacteria count remained relatively low, was longer for $Q_{Tot} = 0.8$ $mL \cdot h^{-1}$ compared to $Q_{Tot} = 0.17$ $mL \cdot h^{-1}$. Future detailed studies of growth kinetics using the FT-μBR will monitor the pre-biofilm sessile bacteria population sizes in time within the template region for different conditions, such as flow rates, concentrations, surface materials and temperatures.

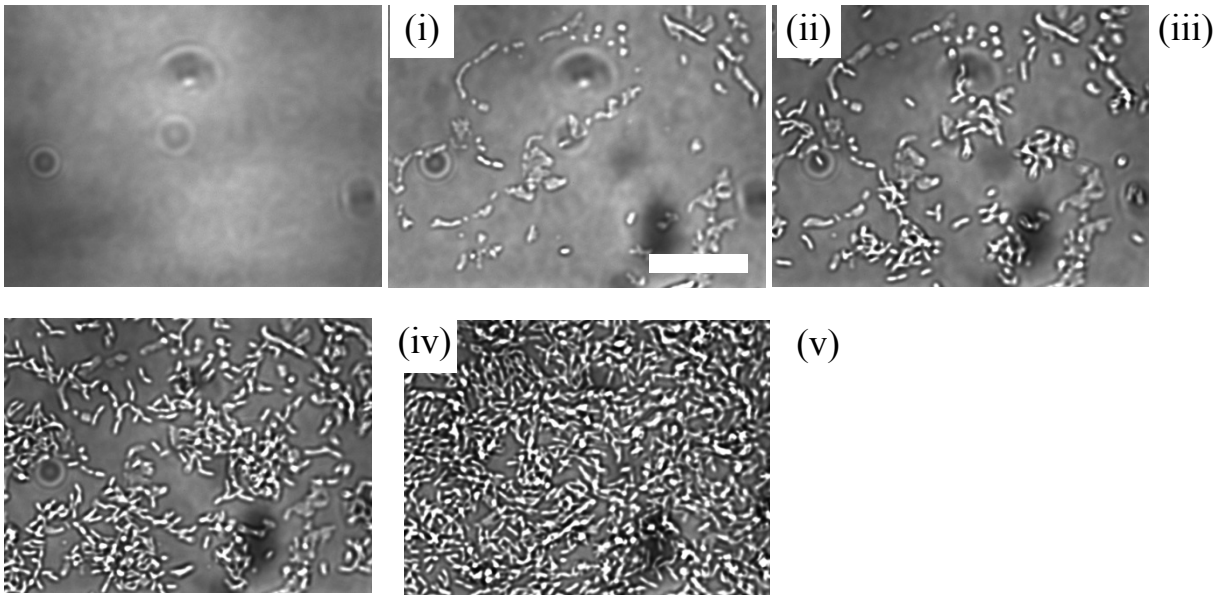

Fig. 8a High resolution bright field images of the sessile bacteria immediately following inoculation at times $t_i < 0$ h (pre-inoculation), $t_{ii} = 0$ h, $t_{iii} = 21$ h and $t_{iv} = 30$ h, $t_v = 40$ h for $Q_T = 0.8 mL \cdot h^{-1}$. The figure (v) is representative of an overcrowded field of view, for which bacterial counting was not possible. Images were acquired using 100x objective. Scale bar is 2 µm and the field of view in all images is 65 μm^2.

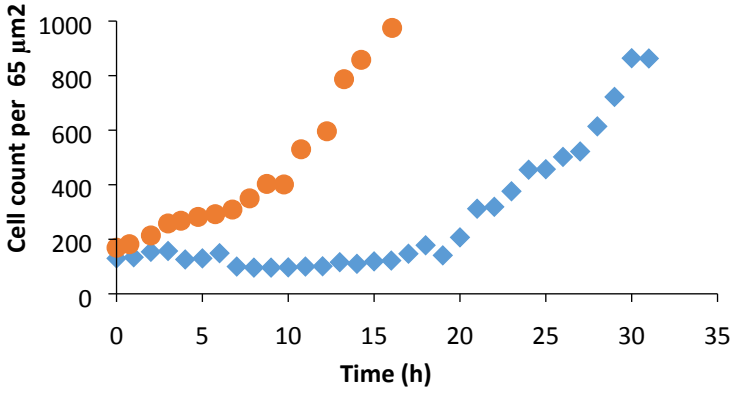

Fig. 8b Cell counting during the pre-biofilm phase for $Q_{Tot} = 0.17$ $mL \cdot h^{-1}$ (orange circles) and $Q_{Tot} = 0.8$ $mL \cdot h^{-1}$ (blue diamonds). Data were automatically acquired each every hour and cell counting was accomplished using automated detection and counting macros.